Available online at www.sciencedirect.com
ScienceDirect
ELSEVIER
Ultramicroscopy 107 (2007) 1033–1041
ultramicroscopy
www.elsevier.com/locate/ultramic

Wetting study of patterned surfaces for superhydrophobicity

Bharat Bhushan*, Yong Chae Jung

Nanotribology Laboratory for Information Storage and MEMS/NEMS (NLIM), 201 W. 19th Avenue, The Ohio State University, Columbus, OH 43202-1107, USA

Abstract

Superhydrophobic surfaces have considerable technological potential for various applications due to their extreme water-repellent properties. A number of studies have been carried out to produce artificial biomimetic roughness-induced hydrophobic surfaces. In general, both homogeneous and composite interfaces are possible on the produced surface. Silicon surfaces patterned with pillars of two different diameters and heights with varying pitch values were fabricated. We show how static contact angles vary with different pitch values on the patterned silicon surfaces. Based on the experimental data and a numerical model, the trends are explained. We show that superhydrophobic surfaces have low hysteresis and tilt angle. Tribological properties play an important role in many applications requiring water-repellent properties. Therefore, it is important to study the adhesion and friction properties of these surfaces that mimic nature. An atomic/friction force microscope (AFM/FFM) is used for surface characterization and adhesion and friction measurements.

Keywords: Hydrophobic; Lotus effect; Air pocket; Contact angle; Hysteresis; Tilt angle

1. Introduction

Superhydrophobic surfaces are of considerable interest for various technological applications due to their extreme water-repellent properties. Advances in nanotechnology, including micro/nanoelectromechanical systems (MEMS/NEMS), have stimulated the development of new materials and design of surfaces which should require hydrophobic surfaces and interfaces with low adhesion and friction. One of the crucial surface properties for materials in micro/nanoscale applications is water repellency, non-wetting or hydrophobicity. It is also usually desirable to reduce wetting and increase liquid slip in liquid flow applications. Hydrophilic or hydrophobic properties of a surface (wettability) are characterized by the static contact angle, or simply contact angle, made between a water droplet and a surface. A surface is hydrophilic if the value of the contact angle is less than 90°, whereas the surface is hydrophobic if the value of the contact angle is greater than 90°. Surfaces with the contact angle between 150° and 180° are called superhydrophobic. The contact angle depends on several factors, such as surface energy, roughness, the manner of surface preparation, and surface cleanliness [1–5]. Hydrophobic (water-repellent) surfaces can be constructed by using low surface energy materials, coatings such as polytetrafluoroethylene or wax. The hydrophobicity of a surface can also be increased by increasing the surface area by increasing surface roughness and/or creation of air pockets. Air may be trapped in the cavities of a rough surface, resulting in a composite solid–air–liquid interface, as opposed to the homogeneous solid–liquid interface [6–9].

Superhydrophobic surfaces have very low water contact angle hysteresis, the difference between the advancing and receding contact angles. If additional liquid is added to a sessile drop, the contact line advances and an advancing contact angle is measured. Alternatively, if liquid is removed from the drop, the contact angle decreases to a receding value before the contact retreats. For a droplet moving along the solid surface, the contact angle at the front of the droplet (advancing contact angle) is greater than that at the back of the droplet (receding contact angle), due to roughness and surface heterogeneity, resulting in the contact angle hysteresis. In addition to high contact angle, another wetting property of interest for

*Corresponding author. Tel.: +1 614 292 0651; fax: +1 614 292 0325.
E-mail address: Bhushan.2@osu.edu (B. Bhushan).

0304-3991/$ - see front matter © 2007 Elsevier B.V. All rights reserved.
doi:10.1016/j.ultramic.2007.05.002

liquid flow applications is a very low water roll-off angle, which denotes the angle to which a surface may be tilted for roll off of water drops (i.e., very low water contact angle hysteresis) [10,11].

In the past decade, many researchers have paid attention to the study of hydrophobic materials that can be found in nature. The leaf surfaces of hundreds of different plant species have been studied to examine the effect of roughness on hydrophobicity [12,13]. Among them are the leaves of water-repellent plants such as *Nelumbo nucifera* (lotus) and *Colocasia esculenta*, which have high contact angles with water and show strong self-cleaning properties known as the 'lotus effect' [14]. The two leaf surfaces are covered with micro- and nanobumps which increase roughness. These bumps are covered with a hydrophobic wax. For lotus leaf, the combination of wax and bumps give a contact angle of 162° [12]. Recent studies have been carried out to fully characterize the leaf surfaces on the micro- and nanoscale while separating out the effects of the micro- and the nanobumps, and the wax (crystals that are a mixture of large hydrocarbon molecules, measuring about 1 nm in diameter) of hydrophobic leaves on the hydrophobicity [15,16]. By learning from what is found in nature, we can tailor surfaces to mimic those same properties. Creating roughness on materials such as polymers, and studying their surface properties will lead to successful implementation in applications where water repellency is important.

A number of studies have been carried out to produce artificial biomimetic roughness-induced hydrophobic surfaces [17–25]. Recent studies have investigated metastability of artificial superhydrophobic surfaces. Based on modeling and experiments, it has been shown that whether the interface is homogeneous or composite may depend on several factors, such as the distribution of the bumps present on the surface [26–31].

In a previous paper, we showed whether nanostructures or microstructures or their certain combination on the surface are required for superhydrophobicity. For both hydrophilic and hydrophobic surfaces, contact angle increases with an increase of air pocket formation for both smooth and rough surfaces. To create superhydrophobic surfaces, it is important that they are able to form a stable composite interface with air pockets between solid and liquid. As shown in Fig. 1, micropatterned sample (coated PMMA Lotus) has a higher roughness factor than one of the nanopatterned sample (coated PMMA LAR) but with similar contact angle. This observation suggests that nanopatterned sample benefits from air pocket formation. The second nanopatterned sample (coated PMMA HAR) has the highest roughness factor as well as contact angle, as expected. The measured contact angle of this nanopatterned sample is higher than the calculated values using Wenzel equation. These observations suggest that nanopatterns benefit from air pocket formation [32].

Previous experiments are not conclusive regarding the optimization of distribution of bumps present on the surface. The relationship of air pocket formation and geometric

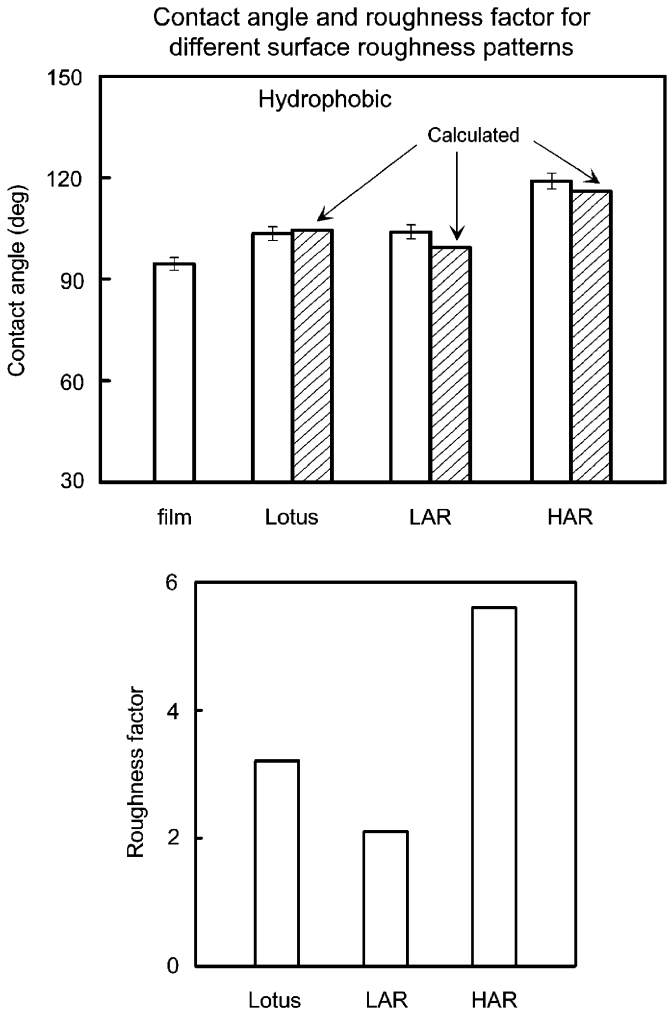

Fig. 1. Bar chart showing the contact angles and roughness factors for different roughness patterns on PMMA polymers coated with a self-assembled monolayer of perfluorodecyltriethoxysilane (PFDTES). Contact angle data, both measured and calculated using Wenzel's equation are shown. Roughness factors were calculated using surface pattern.

parameters needs to be shown. This information is critical in designing a superhydrophobic surface for applications which require water repellency. In this study, numerical models which provide relationships between a rough surface and contact angle using Wenzel and Cassie–Baxter equations are first discussed. The role of patterned surfaces with different pitch between the pillars is examined by measuring their static contact angle. Experiments are also conducted to measure the hysteresis and tilt angles on a given rough hydrophobic surface made of silicon material. We compare the experimental measurements with the numerical models for the static contact angles.

2. Experimental details

2.1. Instrumentation

The static- and dynamic contact angles, a measure of surface hydrophobicity, were measured using a Rame-Hart

model 100 contact angle goniometer and water droplets of deionized water. For the measurement of static contact angle of patterned surfaces, the droplet size should be small but larger than dimension of the structures present on the surfaces. Droplets of about 5 μL in volume (with diameter of a spherical droplet about 2.1 mm) were gently deposited on the substrate using a microsyringe for the static contact angle. The receding contact angle was measured by the removal of water from a DI water sessile drop (~5 μL) using a microsyringe. The advancing contact angle was measured by adding additional water to the sessile drop (~5 μL) using the microsyringe. The contact angle hysteresis was calculated by the difference between the measured advancing and receding contact angles. The tilt angle was measured by a simple stage tilting experiment with the droplets of 5 μL volume. All measurements were made by five different points for each sample at $22 \pm 1\,^{\circ}C$ and $50 \pm 5\%$ RH. The measurements were reproducible to within $\pm 3^{\circ}$.

For surface roughness, an optical profiler (NT-3300, Wyko Corp., Tuscon, AZ) was used for different patterned surface structures. A scan size of 100 μm × 90 μm was used to scan the patterned surface. For adhesion and friction measurements, a commercial AFM (D3100, Nanoscope IIIa controller, Digital Instruments, Santa Barbara, CA) was used. Adhesion and friction were measured using a 15 μm radius borosilicate ball. A large tip radius was used to measure contributions from patterned surfaces. Friction force was measured under a constant load using a 90° scan angle at a velocity of 100 μm/s in 50 μm. Adhesive force was measured using the single point measurement of a force calibration plot [3–5,33].

2.2. Samples

Single-crystal silicon (Si) was used in this study. Silicon material has traditionally been the most commonly used structural material for micro/nanocomponents [34]. Hydrophilic surfaces can be produced by using silicon material. Furthermore, Si structure can be made hydrophobic by coating with a self-assembled monolayer (SAM). For patterned Si, two series of nine samples each were fabricated using photolithography [35]. Series 1 has 5-μm diameter and 10-μm height flat-top, cylindrical pillars with different pitch values (7, 7.5, 10, 12.5, 25, 37.5, 45, 60, and 75 μm), and series 2 has 14-μm diameter and 30-μm height flat-top, cylindrical pillars with different pitch values (21, 23, 26, 35, 70, 105, 126, 168, and 210 μm). The pitch is the spacing between the centers of two adjacent pillars. The Si chosen were initially hydrophilic, so to obtain a sample that is hydrophobic, a SAM of 1, 1, -2, 2, -tetrahydroperfluorodecyltrichlorosilane (PF_3) was deposited on the sample surfaces using vapor phase deposition technique [35]. PF_3 was chosen because of the hydrophobic nature of the surface.

3. Results and discussion

3.1. Surface characterization using an optical profiler

An optical profiler was used to measure the surface topography of the patterned surfaces. One sample each from the two series was chosen to characterize the surfaces. Two different surface height maps can be seen for the patterned Si in Fig. 2. In each figure, a 3D map and a flat map along with a 2D profile in a given location of the flat

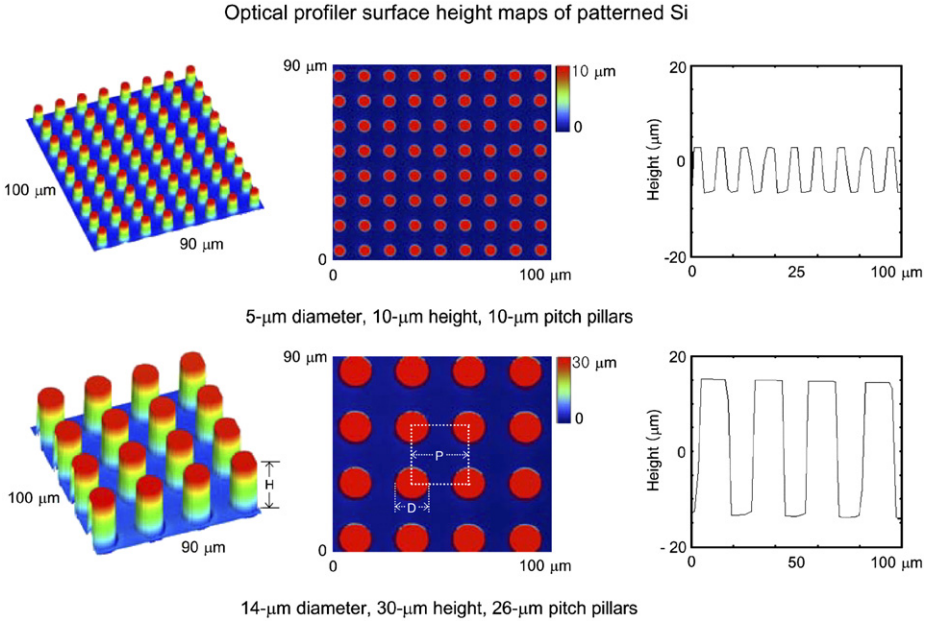

Fig. 2. Surface height maps and 2D profile of the patterned Si surfaces using an optical profiler. The diameter and height of the pillar are *D* and *H*, respectively. The pitch of the pillars is *P*.

3D map are shown. A scan size of 100 μm × 90 μm was used to obtain a sufficient amount of pillars to characterize the surface but also to maintain enough resolution to get an accurate measurement.

The images found with the optical profiler indicate that the flat-top, cylindrical pillars on the Si surface are distributed on the entire surface. These pillars were distributed in a square grid with different pitch values. Roughness factors for these surfaces were calculated as a ratio of the solid–liquid area to its projected area on a flat surface (roughness factor $= 1 + \pi DH/P^2$). Table 1 shows these quantities for the surfaces referred to as series 1 (5-μm diameter, 10-μm height pillars) and series 2 (14-μm diameter, 30-μm height pillars). When compared, it can be seen that the roughness factors for series 1 are similar to those for series 2.

3.2. Contact angle analysis

We consider a rough solid surface with a typical size of roughness structure, smaller than the size of the droplet (typically on the order of few hundred microns or larger). For a droplet in contact with a rough surface without air pockets, referred to as homogeneous interface, the contact angle is given as [6]

$$\cos\theta = R_f \cos\theta_0, \tag{1}$$

where θ is the contact angle for rough surface, θ_0 is the contact angle for smooth surface, and R_f is a roughness factor defined as a ratio of the solid–liquid area A_{SL} to its projection on a flat plane, A_F

$$R_f = \frac{A_{SL}}{A_F}. \tag{2}$$

The model predicts that roughness enhances hydrophobicity if θ_0 is greater than 90°. If θ_0 is less than 90° then the contact angle for the rough surface will decrease with increasing R_f.

For a rough surface, a wetting liquid will be completely absorbed by the rough surface cavities while a non-wetting liquid may not penetrate into surface cavities, resulting in the formation of air pockets, leading to a composite solid–air–liquid interface. Cassie and Baxter [7] extended Wenzel equation for the composite interface, which was originally developed for the homogeneous solid–liquid interface. For this case, there are two sets of interfaces: a solid–liquid interface with the ambient environment surrounding the droplet and a composite interface involving liquid–air and solid–air interfaces. In order to calculate the contact angle for the composite interface, Wenzel equation can be modified by combining the contribution of the fractional area of wet surfaces and the fractional area with air pockets ($\theta = 180°$)

$$\begin{aligned}\cos\theta &= R_f f_{SL}\cos\theta_0 - f_{LA} \\ &= R_f - f_{LA}(R_f\cos\theta_0 + 1),\end{aligned} \tag{3}$$

where f_{SL} and f_{LA} are fractional flat geometrical areas of the solid–liquid and liquid–air interfaces under the droplet, respectively.

We consider a geometry of flat-top, cylindrical pillars of diameter D, height H, and pitch P distributed in a regular square array as shown in Fig. 2. The local deformation for small droplets is governed by surface effects rather than gravity. The curvature of a droplet is governed by the Laplace equation, which relates pressure inside the droplet to its curvature [1]. The curvature is the same at the top and the bottom of the droplet [28,36,37]. For the patterned surface considered here, the maximum droop of the droplet in the recessed region is $(P-D)^2/(8R)$. If the droop is greater than depth of the cavity,

$$(P-D)^2/(8R) \geqslant H \tag{4}$$

the transition from Cassie–Baxter regime to Wenzel regime could occur. For the patterned surfaces and radius of droplet of 1.05 mm used here, Eq. (4) shows that one is always in Cassie–Baxter regime. Next, we obtain Wenzel and Cassie–Baxter equations. For a special case of droplet size much larger than P (of interest in this study), a droplet only contacts the flat-top of the pillars in the composite interface, and the cavities are filled with air. For this case, $f_{LA} = 1 - \pi D^2/4P^2 = 1 - f_{SL}$. Let us further assume that the flat-tops are smooth with $R_f = 1$. Eqs. (1) and (3) for this case reduce to

$$\text{Wenzel}: \quad \cos\theta = \left(1 + \frac{\pi DH}{P^2}\right)\cos\theta_0, \tag{5}$$

$$\text{Cassie and Baxter}: \quad \cos\theta = \frac{\pi D^2}{4P^2}(\cos\theta_0 + 1) - 1. \tag{6}$$

Geometrical values of the flat-top, cylindrical pillars in series 1 and 2 are used for calculating the contact angle for the above-mentioned two cases. Fig. 3 shows the plot of the predicted values of the contact angle as a function of pitch between the pillars for the two cases. With an increase in pitch, the contact angle using Wenzel equation decreases, while the contact angle using Cassie–Baxter equation increases. This indicates that there is a critical pitch below

Table 1
Roughness factor and spacing factor for patterned Si with different pitch values

5-μm diameter, 10-μm height pillars

Pitch (μm)	7	7.5	10	12.5	25	37.5	45	60	75
Roughness factor	4.21	3.79	2.57	2.01	1.25	1.11	1.08	1.04	1.03
Spacing factor	0.71	0.67	0.50	0.40	0.20	0.13	0.11	0.08	0.07

14-μm diameter, 30-μm height pillars

Pitch (μm)	21	23	26	35	70	105	126	168	210
Roughness factor	3.99	3.49	2.95	2.08	1.27	1.12	1.08	1.05	1.03
Spacing factor	0.67	0.61	0.54	0.40	0.20	0.13	0.11	0.08	0.07

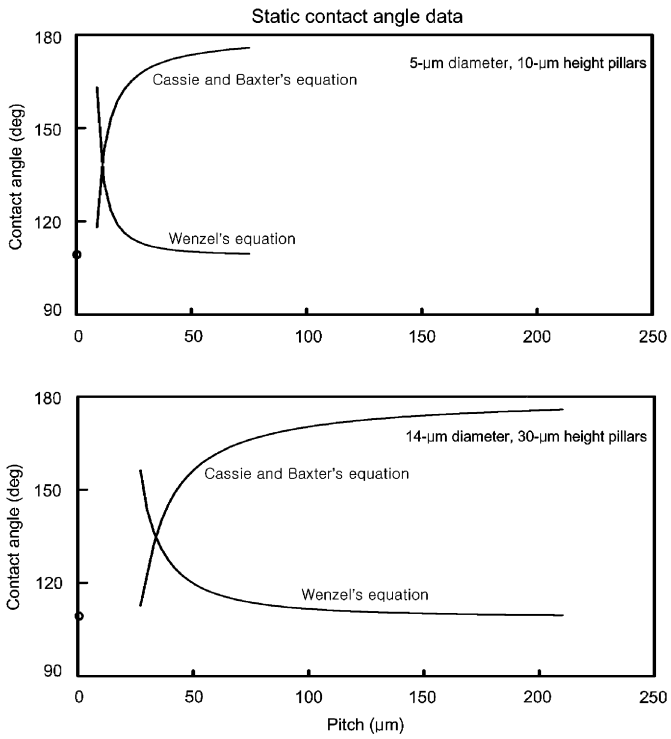

Fig. 3. Plots of the static contact angle as a function of geometric parameters for a given value of θ_0 using Wenzel and Cassie and Baxter equations for two series of the patterned Si with different pitch values, for the case in which cavities form air–liquid interface.

which the composite interface dominates and above which the homogeneous interface dominates the wetting behavior. Therefore, one needs to find the critical point that can be used to design the superhydrophobic surfaces. It should also be noted that even for a case in which the liquid droplet does not contact the bottom of the cavities, if the pitch is large, the water droplet which is in metastable state becomes unstable and the transition from Cassie–Baxter regime to Wenzel regime occurs.

To define transition for patterned surfaces, it is convenient to introduce a non-dimensional parameter, the spacing factor [38]

$$S_f = \frac{D}{P}. \tag{7}$$

The spacing factors for the patterned surfaces were calculated. Table 1 shows these quantities for the surfaces referred to as series 1 (5-μm diameter, 10-μm height pillars) and series 2 (14-μm diameter, 30-μm height pillars). When compared, it can be seen that the spacing factor for series 1 are similar to those for series 2.

3.3. Contact angle measurements

The initial experiment performed on the patterned Si coated with PF_3 was to determine the static contact angle. The contact angles on the prepared surfaces are plotted as a function of pitch between the pillars in Fig. 4(a). The flat

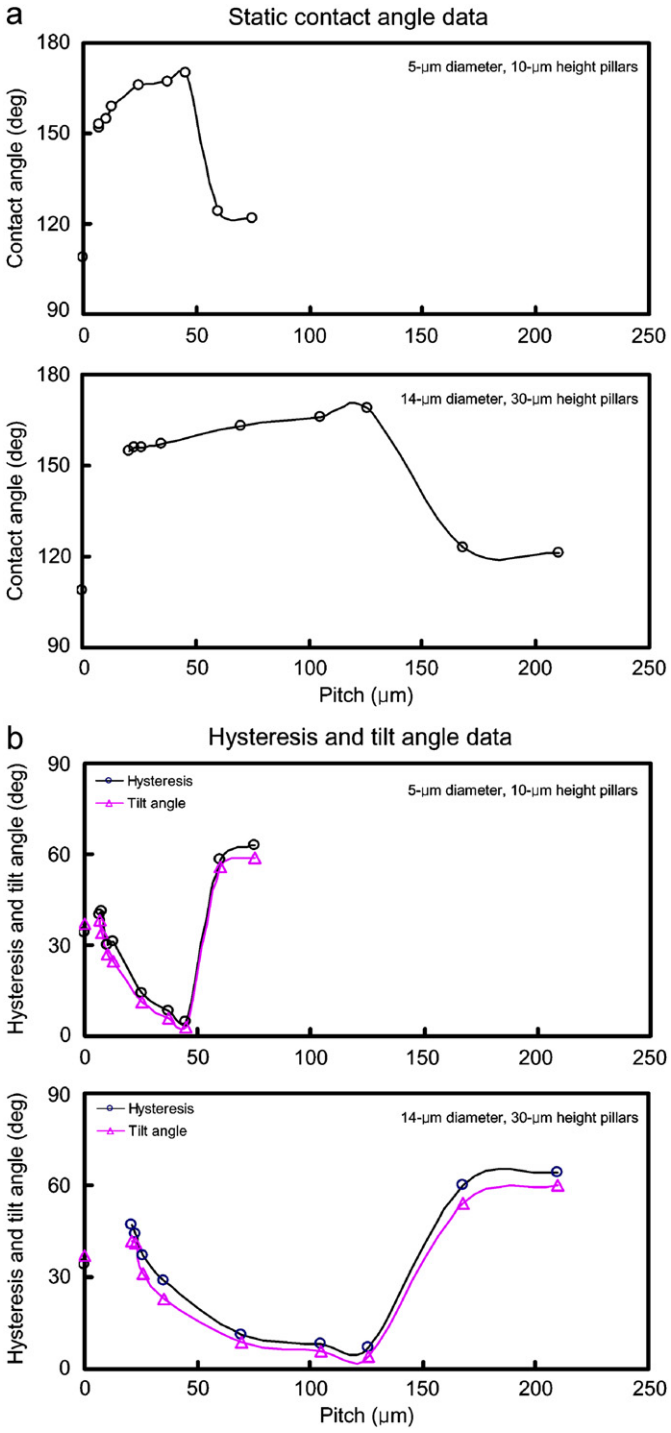

Fig. 4. (a) Static contact angle and (b) hysteresis and tilt angles as a function of geometric parameters for two series of the patterned Si with different pitch values coated with PF_3. Data at zero pitch correspond to a flat Si sample.

Si coated with PF_3 showed the static contact angle of 109°. As the pitch increases up to 45 μm of series 1 and 126 μm of series 2, the static contact angle first increases gradually from 152° to 170°. Then, the contact angle starts decreasing sharply. The highest contact angle for the two patterned surfaces with different pillar sizes corresponds to the

roughness factor of 1.08 and the spacing factor of 0.11 as shown in Table 1. The initial increase in the contact angle is expected to occur because of increase in the roughness factor and formation of composite surface as shown in Fig. 3. Further increase occurs because of increased air–liquid interface as observed by Eq. (6). The decrease in contact angle at higher pitch values results due to the transition from composite interface to solid–liquid interface for the spacing factor between 0.08 and 0.11. Therefore the transition takes place at the critical value of $0.08 < S_f < 0.11$. This suggests that the spacing factor and the fractional solid–liquid area of contact (which is directly related to S_f according to Eq. (7)) are responsible for the transition [38]. In the case of large distances between the pillars, the liquid–air interface can easily be destabilized due to dynamic effects, such as surface waves. This results in the formation of the homogeneous solid–liquid interface. The surfaces formed with larger diameter pillars should have larger pitch to increase the contact angle than those with small diameter pillars.

Fig. 4(b) shows hysteresis and tilt angle as a function of pitch between the pillars. The flat Si coated with PF_3 showed a hysteresis angle of 34° and tilt angle of 37°. The patterned surfaces with low pitch increase the hysteresis and tilt angles compared to the flat surface due to the effect

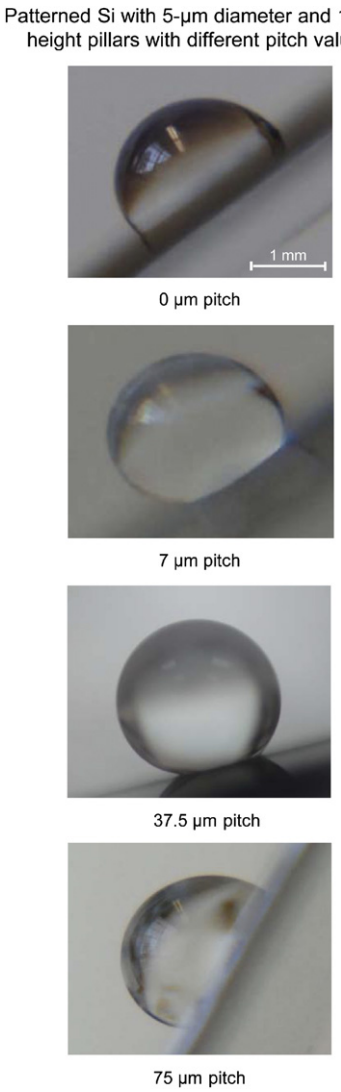

Fig. 5. Droplets on the inclined patterned Si with different pitch values coated with PF_3. The images were taken when the droplet started to move down. Data at zero pitch correspond to a flat Si sample.

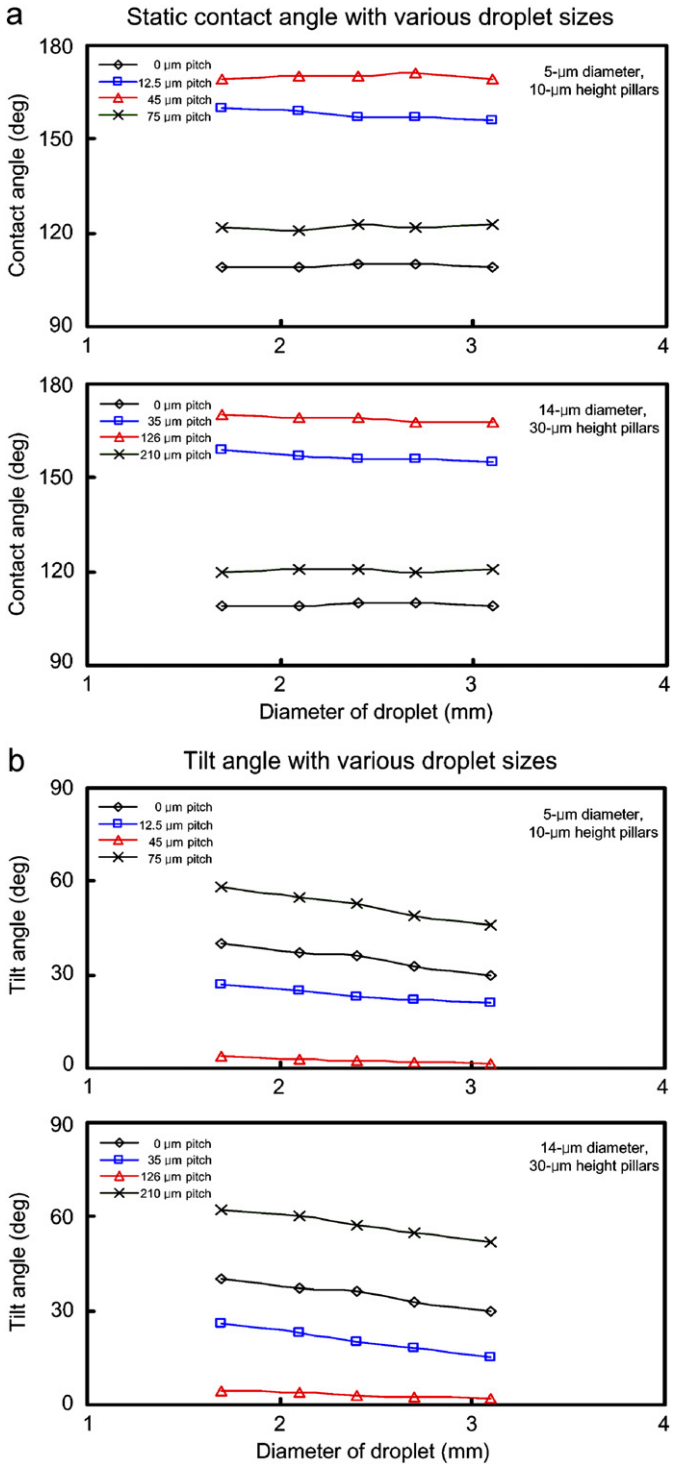

Fig. 6. (a) Static contact angle and (b) tilt angle as a function of the diameter of droplet for two series of the patterned Si with different pitch values coated with PF_3. Data at zero pitch correspond to a flat Si sample.

of sharp edges on the pillars, resulting into pinning [8]. Hysteresis for a flat surface can arise from roughness and surface heterogeneity. For a droplet moving down on the inclined patterned surfaces, the line of contact of the solid, liquid and air will be pinned at the edge point until it will be able to move, resulting into increasing hysteresis and tilt angles. Fig. 5 shows droplets on patterned Si with 5-μm diameter and 10-μm height pillars with different pitch values. The asymmetrical shape of the droplet signifies pinning. The pinning on the patterned surfaces can be observed as compared to the flat surface. The patterned surface with low pitch (7 μm) has more the pinning than the patterned surface with high pitch (37.5 μm), because the patterned surface with low pitch has more sharp edges contacting with a droplet.

For various pitch values, hysteresis and tilt angles show the same trends with varying pitch between the pillars. After an initial increase as discussed above, they gradually decrease with increasing pitch and show an abrupt minimum in the value which has the highest contact angle. The lowest hysteresis and tilt angles are 5° and 3°, respectively, which were observed on the patterned Si with 45 μm of series 1 and 126 μm of series 2. As discussed earlier, an increase in the pitch value allows the formation of composite interface. At higher pitch values, it is difficult to form the composite interface. The decrease in hysteresis and tilt angles occurs due to formation of composite interface at pitch values ranging from 7 to 45 μm in series 1 and from 21 to 126 μm in series 2. The hysteresis and tilt angles start to increase again due to lack of formation of air pockets at pitch values ranging from 60 to 75 μm in series 1 and from 168 to 210 μm in series 2. These results suggest that the air pocket formation and the reduction of pinning in the patterned surface play an important role for a surface with both low hysteresis and tilt angle. Hence, to create superhydrophobic surfaces, it is important that they are able to form a stable composite interface with air pockets between solid and liquid. Capillary waves, nanodroplet condensation, hydrophilic spots due to chemical surface inhomogeneity, and liquid pressure can destroy the composite interface. Nosonovsky and Bhushan [38] suggested that these factors which make the composite interface unstable have different characteristic length scales, so nanostructures or the combination of microstructures and nanostructures is required to resist them.

To study the tilt angle on the flat and patterned surfaces, experiments with various droplet sizes (volume of 3 to 15 μL corresponding to diameters of spherical droplets from 1.7 to 3.1 mm) were performed. Fig. 6 shows the results of the static contact angle and tilt angle for different patterned surfaces with various droplet sizes. For the static contact angle as shown in Fig. 6(a), as the droplet size is increased the contact angle does not significantly change for all samples. For the tilt angle as shown in Fig. 6(b), as the droplet size is increased the tilt angle decreases for all samples. This indicates that smaller droplets have more resistance against moving down, because interfacial forces due to the surface tension are higher than gravitational forces, and vice versa.

3.4. Adhesive force and coefficient of friction

For adhesive force and coefficient of friction, due to the problem of tip radius being smaller than pitch of some of the patterned surfaces, only surfaces with 5-μm diameter and 10-μm height pillars and different pitch values from 0 to 12.5 μm, were used to see the change in adhesion and friction for each type of surface structure. The results from varying pitch on the patterned Si are summarized in Fig. 7. Reproducibility for both adhesive force and coefficient of friction is ±3% for all measurements. For these experiments, only the 15 μm radius tip was used to study the effect from the pillars on the patterned surfaces.

With the presence of a thin liquid film, such as a lubricant or adsorbed water layer at the contact interface, wetting results in the formation of menisci at the interface between two hydrophilic surfaces during sliding contact due to surface energy effects, which increases adhesion and friction. For an idealized case of a smooth sphere in contact with a smooth surface, the meniscus force, F_m, is

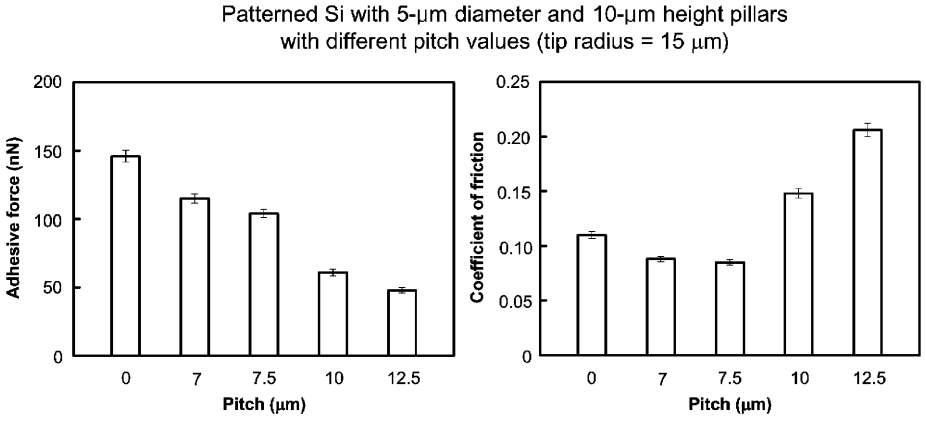

Fig. 7. Adhesive force and the coefficient of friction for the patterned Si with different pitch values coated with PF_3. All measurements were made using a 15 μm radius borosilicate tip. Data at zero pitch correspond to a flat Si sample.

given by the expression

$$F_m = 2\pi R\gamma(\cos\theta_1 + \cos\theta_2), \quad (8)$$

where R is the radius of the sphere, γ is the surface tension of the liquid, and θ_1 and θ_2 are the contact angles of the liquid on the two solid surfaces [3–5]. For the wet interfaces during normal pull and lateral sliding, adhesive and friction forces increase, respectively.

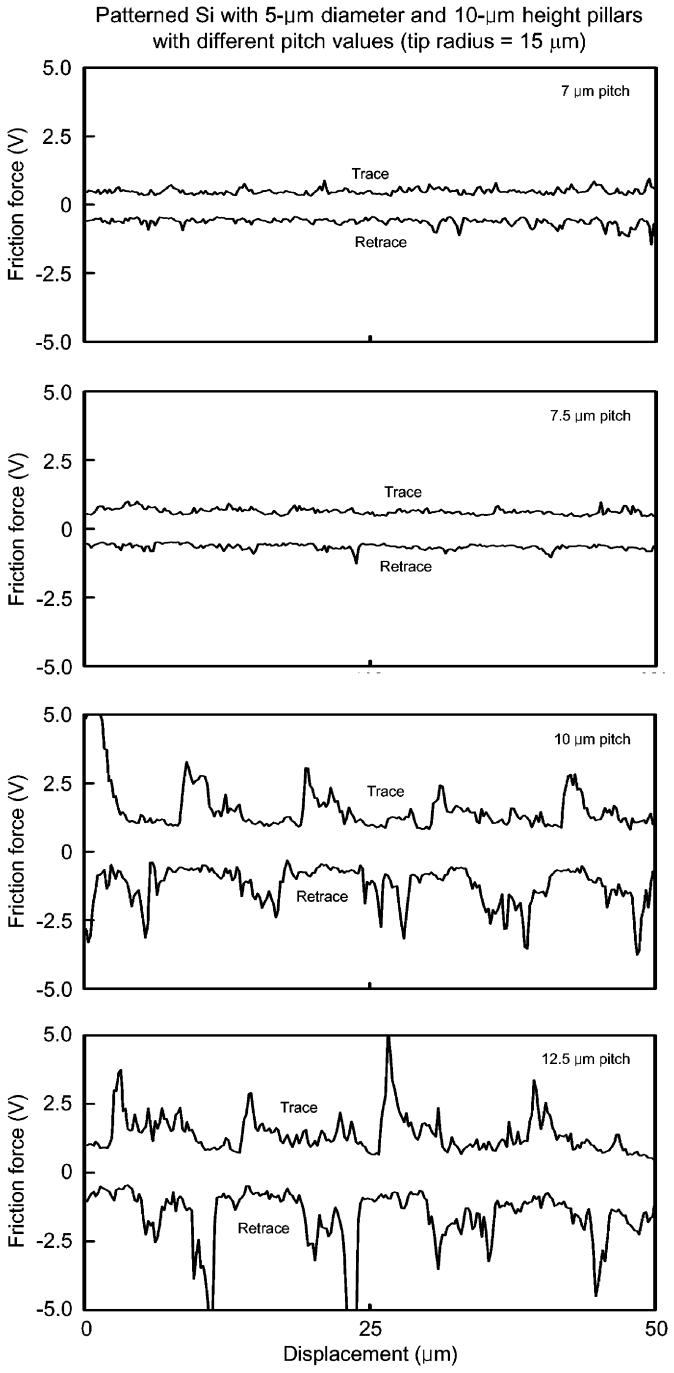

Fig. 8. Two-dimensional profiles of friction forces for the patterned Si with different pitch values coated with PF_3. 'Sick-slip' phenomenon was found in the patterned surfaces of 10 and 12.5 μm pitch. Trace and retrace are two scan directions used in AFM measurements.

As shown in Fig. 7, for the adhesive force values there is a decrease when the pitch increases because the tip traveling between the pillars results in the decreased contact area, responsible for decreased adhesive force. Coefficient of friction data also follows a similar trend to the adhesion data for the pitch values from 0 to 7.5 μm. There is a decrease when the pitch increases due to the decreased contact area between the tip and pillars. However, an abrupt increase in coefficient of friction occurs at pitch values of 10 μm or higher. As shown in Fig. 8, when the 15 μm radius tip travels on the patterned Si, the friction force does remain constant as a function of distance in 7 and 7.5 μm pitch value pillars, while it does not remain constant in 10 and 12.5 μm pitch value pillars, and shows oscillations. The mechanism responsible for the obtained trends is 'stick-slip' phenomenon, in which during the stick phase, the friction force builds up to a certain value, and once a large enough force has been applied to overcome the static friction force, slip occurs at the interface [3–5].

4. Conclusions

Based on Wenzel and Cassie–Baxter equations, we have presented design curves to optimize for the contact angle for patterned surfaces with various distributions of geometrical parameters for a large radius of water droplet. The experimental results for the patterned surfaces with different pitch values showed the transition from the composite interface to homogeneous interface. In the case of large distances between the pillars, the liquid–air interface can easily be destabilized due to dynamic effects such as surface waves. A water droplet in state of the composite interface shows significantly less hysteresis and tilt angles compared to a water droplet in state of the homogeneous interface due to low resistance from the air pockets. The pinning of the droplet at the edges of the pillars takes place during the motion of the droplet and thus pinning results in an increase of hysteresis and tilt angles. These results suggest that the air pocket formation and the absence of pinning in the patterned surface play an important role for a superhydrophobic surface. For adhesive force and coefficient of friction, there is a decrease when the pitch increases because the tip traveling between the pillars results in the decreased contact area.

Acknowledgments

Financial support for this project was provided in part by the National Science Foundation (no. ECS-0301056). The authors thank Dr. Patrik Hoffmann and Dr. Laura Barbieri of Ecole Polytechnique Federale de Lausanne (EPFL) Switzerland for sample preparation.

References

[1] A.V. Adamson, Physical Chemistry of Surfaces, Wiley, NY, 1990.
[2] J.N. Israelachvili, Intermolecular and Surface Forces, second ed., Academic Press, London, 1992.

[3] B. Bhushan, Handbook of Micro/Nanotribology, second ed., CRC Press, Boca Raton, FL, 1999.
[4] B. Bhushan, Introduction to Tribology, Wiley, NY, 2002.
[5] B. Bhushan, Nanotribology and Nanomechanics—An Introduction, Springer, Heidelberg, Germany, 2005.
[6] R.N. Wenzel, Ind. Eng. Chem. 28 (1936) 988.
[7] A. Cassie, S. Baxter, Trans. Faraday Soc. 40 (1944) 546.
[8] M. Nosonovsky, B. Bhushan, Microsyst. Technol. 11 (2005) 535.
[9] M. Nosonovsky, B. Bhushan, Microsyst. Technol. 12 (2006) 273.
[10] C.W. Extrand, Langmuir 18 (2002) 7991.
[11] J. Kijlstra, K. Reihs, A. Klami, Colloids Surf. A: Physicochem. Eng. Aspects 206 (2002) 521.
[12] C. Neinhuis, W. Barthlott, Ann. Botany 79 (1997) 667.
[13] P. Wagner, F. Furstner, W. Barthlott, C. Neinhuis, J. Exp. Botany 54 (2003) 1295.
[14] W. Barthlott, C. Neinhuis, Planta 202 (1997) 1.
[15] Z. Burton, B. Bhushan, Ultramicroscopy 106 (2006) 709.
[16] B. Bhushan, Y.C. Jung, Nanotechnology 17 (2006) 2758.
[17] S. Shibuichi, T. Onda, N. Satoh, K. Tsujii, J. Phys. Chem. 100 (1996) 19512.
[18] A. Hozumi, O. Takai, Thin Solid Film 334 (1998) 54.
[19] S.R. Coulson, I. Woodward, J.P.S. Badyal, J. Phys. Chem. B 104 (2000) 8836.
[20] M. Miwa, A. Nakajima, A. Fujishima, K. Hashimoto, T. Watanabe, Langmuir 16 (2000) 5754.
[21] D. Oner, T.J. McCarthy, Langmuir 16 (2000) 7777.
[22] L. Feng, S. Li, Y. Li, H. Li, L. Zhang, J. Zhai, Y. Song, B. Liu, L. Jiang, D. Zhu, Adv. Mater. 14 (2002) 1857.
[23] H.Y. Erbil, A.L. Demirel, Y. Avci, Science 299 (2003) 1377.
[24] K.K.S. Lau, J. Bico, K.B.K. Teo, M. Chhowalla, G.A.J. Amaratunga, W.L. Milne, G.H. Mckinley, K.K. Gleason, Nano Letters 3 (2003) 1701.
[25] Z. Burton, B. Bhushan, Nano Letters 5 (2005) 1607.
[26] J. Bico, U. Thiele, D. Quere, Colloids Surf. A 206 (2002) 41.
[27] A. Marmur, Langmuir 19 (2003) 8343.
[28] A. Lafuma, D. Quéré, Nature Mater. 2 (2003) 457.
[29] N.A. Patankar, Langmuir 19 (2003) 1249.
[30] B. He, N.A. Patankar, J. Lee, Langmuir 19 (2003) 4999.
[31] W. Li, A. Amirfazli, J. Colloid. Interface Sci. 292 (2005) 195.
[32] Y.C. Jung, B. Bhushan, Nanotechnology 17 (2006) 4970.
[33] B. Bhushan, J. Vac. Sci. Technol. B 21 (2003) 2262.
[34] B. Bhushan, Springer Handbook of Nanotechnology, second ed., Springer, Heidelberg, Germany, 2007.
[35] L. Barbieri, Wetting properties of flat-top periodically structured superhydrophobic surfaces, Ph.D. Thesis, EPFL, Lausanne, Switzerland, 2006.
[36] M. Nosonovsky, B. Bhushan, Lotus Effect: Roughness-Induced Superhydrophobicity, in: B. Bhushan (Ed.), Applied Scanning Probe Methods, vol. 7, Springer, Berlin, 2007, pp. 1–40.
[37] M. Reyssat, D. Quéré, personal communications, 2006.
[38] M. Nosonovsky, B. Bhushan, Microelectron. Eng. 84 (2007) 382.